NUMERICAL APPROXIMATION OF A MACROSCOPIC MODEL OF PEDESTRIAN FLOWS

CHRISTOPHE CHALONS*

Abstract. This paper is concerned with the numerical approximation of the solutions of a macroscopic model for the description of the flow of pedestrians. Solutions of the associated Riemann problem are known to be possibly *nonclassical* in the sense that the underlying discontinuities may well violate the Lax inequalities, which makes their numerical approximation very sensitive. This study proposes to extend the Transport-Equilibrium strategy proposed in [2] for computing the nonclassical solutions of scalar conservation laws with an either *concave-convex* or *convex-concave* flux function and supplemented with an *invertible* kinetic function. These strong properties are not fulfilled in the present setting since both the flow function admits several inflection points and the kinetic function is not invertible. We nevertheless succeed in obtaining an efficient numerical scheme. Numerical evidences are proposed.

Key words. macroscopic pedestrian flows, nonclassical shocks in conservation laws, kinetic function, transport-equilibrium schemes

AMS subject classifications. 35L60, 35L65, 35L67, 35R60, 76M25, 76L05

1. Introduction. In this paper, we are interested in the numerical approximation of the weak solutions of a scalar conservation law arising in the description of the flow of pedestrians. The model reads

$$\left\{ \begin{array}{l} \partial_t \rho + \partial_x q(\rho) = 0, \ \ \rho(x,t) \in \mathbb{R}, \ \ (x,t) \in \mathbb{R}\times]0,+\infty[, \\ \rho(x,0) = \rho_0(x), \ \ x \in \mathbb{R}, \end{array} \right. \tag{1.1}$$

where $\rho \geq 0$ is the pedestrian density and $q : \mathbb{R}^+ \to \mathbb{R}^+$ is the flow function. Generally speaking, the solutions of (1.1) may develop discontinuities in finite time, however are smooth the function q and the initial data ρ_0. Then, it turns out that the weak solutions (in the integral sense) of (1.1) are not uniquely determined by initial data ρ_0. In order to single out the solution of interest, various admissibility principles are used in the literature, depending on the geometric properties of the function q. For instance, one may ask the discontinuities of (1.1) separating two constant states ρ_- and ρ_+ and propagating with speed σ given by the Rankine-Hugoniot relation $\sigma = [q(\rho_+) - q(\rho_-)] \, / \, [\rho_+ - \rho_-]$, to obey Oleinik's inequalities :

$$\frac{q(\rho) - q(\rho_-)}{\rho - \rho_-} \geq \frac{q(\rho_+) - q(\rho_-)}{\rho_+ - \rho_-}, \ \text{ for all } \rho \text{ between } \rho_- \text{ and } \rho_+. \tag{1.2}$$

Observe that (1.2) coincides with Liu's criterion [15] for scalar conservation laws. Another usual criterion is based on the Lax inequalities :

$$q'(\rho_-) \geq \sigma \geq q'(\rho_+). \tag{1.3}$$

In particular, we note that Oleinik's inequalities (1.2) imply the Lax inequalities (1.3). Discontinuities satisfying (1.3) are said to be *compressive*.
When q is convex (or concave), conditions (1.2) and (1.3) are equivalent and select a unique solution of the so-called Riemann problem associated with (1.1), *i.e.* problem

*Université Paris 7 & Laboratoire JLL, U.M.R. 7598, Boîte courrier 187, 75252 Paris Cedex 05, France. (chalons@math.jussieu.fr).

(1.1) when considering the particular initial data

$$\rho_0(x) = \begin{cases} \rho_l & \text{if} \quad x < 0, \\ \rho_r & \text{if} \quad x > 0. \end{cases} \tag{1.4}$$

If q is neither convex nor concave, Oleinik's inequalities still lead to a unique solution and following [11], this solution is called *classical solution*. Recall that the classical solution of (1.1)-(1.4) satisfies a maximum principle, which means that for all $x \in \mathbb{R}$ and $t \geq 0$, $\rho(x,t) \in [\min(\rho_l, \rho_r), \max(\rho_l, \rho_r)]$.
However, PDE (1.1) naturally generates shock waves violating the Lax inequalities (1.3) (and then Oleinik's inequalities) when q fails to be convex (or concave), and these are to be considered. They are referred in [11] as *undercompressive shocks*, or as *nonclassical shocks* and a solution which contains such a shock is said to be *nonclassical*. The uniqueness of the *nonclassical* weak solution of problem (1.1)-(1.4) is generally restored by means of a *kinetic relation* imposed along each undercompressive discontinuity connecting a left state ρ_- to a right state ρ_+. It takes the form $\rho_+ = \psi(\rho_-)$ where ψ is the so-called *kinetic function*. In this context, note that the solution no longer obeys a *maximum principle* and has in general a total variation larger than its initial data. We refer the reader to [11] for a general theory of the classical and nonclassical solutions.

The precise model we consider in this study was introduced recently by Colombo and Rosini [7]. It is based on the well-known Lighthill-Whitam [14] and Richards [16] model and takes the form of (1.1) as an immediate consequence of two basic assumptions, namely the conservation of the total number of pedestrians and a given speed law which depends on the density $\rho \in [0, R]$ only (R denotes the maximal density). However, this model was first dedicated to car flows and so it is not able to reproduce important features of pedestrian flows, at least when considering typical concave increasing - decreasing flow functions. For instance let us mention the *overcompression* phenomenon in a crowd or the fall of pedestrians in the outflow through a door of a crowd in panic. In order to overcome this difficulty, Colombo and Rosini [7] first proposed to modify the typical shape of the flow function q by introducing another characteristic density $R^\star > R$ for the maximal density in exceptional situations of panic. The flow function now looks like a concave - convex and increasing - decreasing function on $[0, R]$ and a convex - concave and increasing - decreasing function on $[R, R^\star]$ (like in Figure 2.1 - Left below). In particular, discontinuities satisfying the usual Rankine-Hugoniot condition but violating the standard admissibility conditions such as the Lax inequalities (1.3) are present in the model. Then, the same authors defined a unique Riemann solver using such undercompressive shocks. The main motivation in considering nonclassical solutions is to allow panic states ($\rho \in]R, R^\star]$) to appear in a calm situation ($\rho \in [0, R]$), because of a sharp increase in the density for instance. Note that the *maximum principle* in classical solutions prevents such panic situations from arising.

From a numerical point of view, the approximation of nonclassical solutions is known to be very challenging and still constitutes (generally speaking) an open problem nowadays (see for instance [8], [9], [12], [3], [4], [5], but also [1] and the references within). The main difficulty is related to the respect of the kinetic relation at the discrete level. Very recently, a new efficient numerical strategy has been proposed in [2] for computing nonclassical solutions of scalar conservation laws in the situation when the flux function is concave-convex or convex-concave and, in an important way, when the kinetic function is an invertible function from $\mathbb{R}$ to $\mathbb{R}$. The algorithm proposed in [2] heavily relies on the latter property. Roughly speaking, the corresponding

finite volume scheme is based on two steps, namely an *Equilibrium step* which treats each undercompressive shock as a non-moving discontinuity, and a *Transport step* for propagating these discontinuities. Here, it turns out that on the one hand the flow function q admits several inflexion points, and on the other hand the kinetic function ψ (defined in (3.2) and represented on Figure 3.1 - Right) is neither defined on the whole domain $\mathbb{R}$ nor invertible. In this paper, we thus propose to adapt the Transport-Equilibrium scheme developed in [2] to the present setting. The resulting scheme still provides numerical solutions in full agreement with exact ones.

2. Governing equation and closure relation. In this section, we present the model we use for describing the flow of pedestrians. Our approach considers the well-known Lighthill-Whitam [14] and Richards [16] model as a basic model. According to (1.1), it takes the form

$$\left\{ \begin{array}{l} \partial_t \rho + \partial_x q(\rho) = 0, \quad q(\rho) = \rho v(\rho), \ \ (x,t) \in \mathbb{R} \times]0, +\infty[, \\ \rho(x,0) = \rho_0(x), \ \ x \in \mathbb{R}, \end{array} \right. \tag{2.1}$$

where ρ denotes the pedestrian density, v the pedestrian speed, and q the flux function. This equation expresses the conservation of the number of pedestrians in the space domain, while the speed v is assumed to depend only on the density ρ. Let us recall that this model was first dedicated to car flows and so is not *a priori* in position to account for specific features of human flows, like the *overcompression* phenomenon due to panic for instance. That is the reason for which, following [7], we introduce two remarkable values R and $R^\star$ ($R < R^\star$) for the density ρ. The first one represents a natural bound of ρ in situations with little or not panic ($\rho \in [0, R]$), and the second one is a maximal value of ρ in situations of great panic ($\rho \in]R, R^\star]$). In each of these two regions, the flow function q typically increases at first and then decreases. More precisely, the following assumptions are made in [7] :

$$\left\{ \begin{array}{ll} \text{(i)} & q : [0, R^\star] \to [0, +\infty[\text{ belongs to } \mathcal{C}^0([0, R^\star]) \cap \mathcal{C}^2([0, R[\cup]R, R^\star]), \\ \text{(ii)} & q(\rho) = 0 \text{ if and only if } q \in \{0, R, R^\star\}, \\ \text{(iii)} & q' \text{ is bounded and vanishes exactly twice, once in } R_M \in]0, R[, \text{ and once in} \\ & R_M^\star \in]R, R^\star[, \\ \text{(iv)} & q \text{ has at most one inflection point } R_I \in]R_M, R[, \text{ and at most another one} \\ & R_I^\star \in]R, R_M^\star[. \end{array} \right. \tag{2.2}$$

For the sake of illustration, we already mention that the numerical experiments in the Section 5 are performed with

$$q(\rho) = -\rho(\rho - R)^2(\rho - R^\star), \quad R = 2, \quad R^\star = 3, \tag{2.3}$$

so that

$$R_M \simeq 0.5570, \quad R_M^\star \simeq 2.6930, \quad R_I \simeq 1.1208, \quad R_I^\star \simeq 2.3792. \tag{2.4}$$

Both the graphs of this flux function $\rho \to q(\rho)$ and the corresponding speed function $\rho \to v(\rho) = q(\rho)/\rho$ are plotted on Figure 2.1. In particular, note that the speed function $\rho \to v(\rho)$ is decreasing on $[0, R]$, while it is first increasing, then decreasing on $[R, R^\star]$.

3. The Riemann solver. This section aims at defining a (unique) weak solution of (2.1)-(2.2) defined for all $(x,t) \in \mathbb{R} \times \mathbb{R}^{+,*}$ when initial data $x \to \rho_0(x)$ is only made

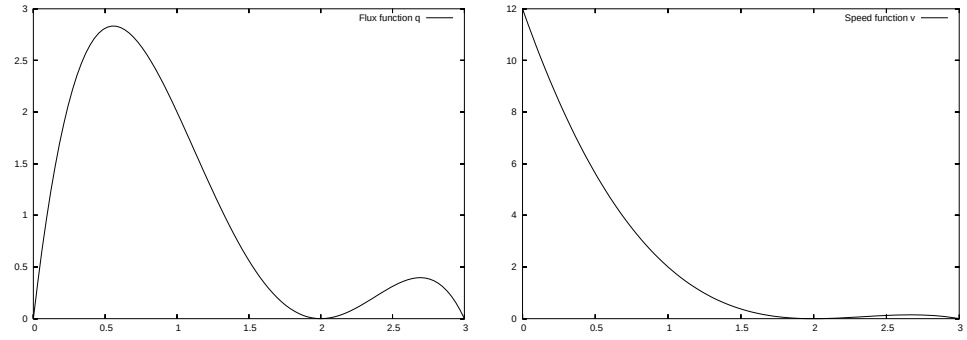

FIG. 2.1. *Closure relations : $\rho \to q(\rho)$ (Left) and $\rho \to v(\rho) = q(\rho)/\rho$ (Right)*

of two constant states ρ_l and ρ_r, unspecified in $[0, R^\star]$ and separated by a discontinuity located at $x = 0$:

$$\rho_0(x) = \begin{cases} \rho_l & \text{if} \quad x < 0, \\ \rho_r & \text{if} \quad x > 0. \end{cases} \tag{3.1}$$

With this in mind and following [7] and [11], we define two functions $\psi : [0, R^\star] \to [R, R^\star]$ and $\Phi : [0, R] \to [0, R]$ related to the graph of the function q in the (ρ, q)-plane. We proceed as follows : as soon as it is possible, $\psi(\rho)$ is such that the line that passes through the points with coordinates $(\rho, q(\rho))$ and $(\psi(\rho), q(\psi(\rho)))$ is tangent to the graph of the function q at point $(\psi(\rho), q(\psi(\rho)))$, while $\Phi(\rho)$ is such that this line intersects the curve $q = q(\rho)$ at a further point with coordinates $(\Phi(\rho), q(\Phi(\rho)))$; otherwise, these functions are extended by continuity as follows :

$$\psi(\rho) = \begin{cases} r \text{ such that } q'(r) = \frac{q(r)-q(\rho)}{r-\rho} & \text{if possible,} \\ R_I^\star & \text{if } \rho = R_I^\star, \\ R \text{ or } R^\star & \text{otherwise,} \end{cases} \tag{3.2}$$

and

$$\Phi(\rho) = \begin{cases} r \text{ such that } \frac{q(r)-q(\rho)}{r-\rho} = \frac{q(\rho)-q(\psi(\rho))}{\rho-\psi(\rho)} & \text{if possible,} \\ 0 & \text{otherwise.} \end{cases} \tag{3.3}$$

Note that the required continuity property of the function $\rho \to \psi(\rho)$ actually selects a unique value between R and $R^\star$ in the last situation of (3.2) (see [7] for an example). Moreover, the inflection point $R_I^\star$ does not necessarily exist in (2.2)-(iv). In this case, we set $R_I^\star = R$.

Figure 3.1 is concerned with the functions ψ and Φ when q is given by (2.3). On the left, we have plotted both the function q and line L_0 passing through the points with coordinates $(0, q(0) = 0)$, $(\Phi(0), q(\Phi(0)))$ and $(\psi(0), q(\psi(0)))$. Of course, we observe that L_0 is actually tangent to the graph of the function q at point $(\psi(0), q(\psi(0)))$ and cuts this graph at point $(\Phi(0), q(\Phi(0)))$. From a numerical point of view, we have

$$\psi(0) = \frac{8}{3} \simeq 2.6667 \quad \text{and} \quad \Phi(0) = \frac{5}{3} \simeq 1.6667. \tag{3.4}$$

On the right are represented the functions $\rho \to \psi(\rho)$ and $\rho \to \Phi(\rho)$ on their whole interval of definition.

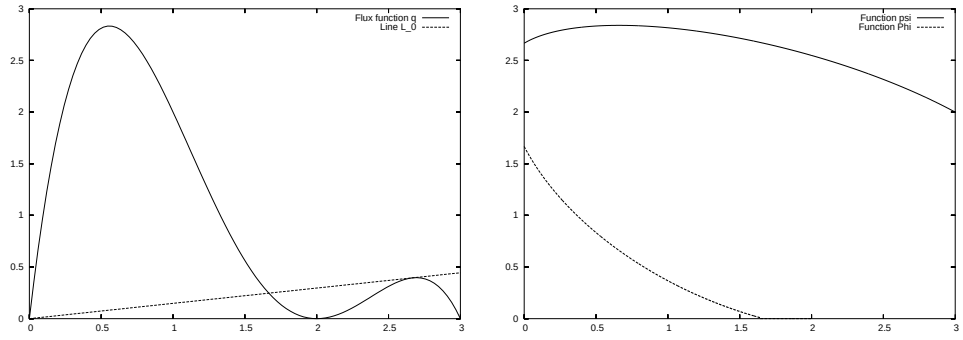

FIG. 3.1. *Function q and line L_0 (Left) - Functions ψ and Φ (Right)*

The next theorem, first stated and proved by Colombo and Rosini [7], now defines a unique Riemann solver for (2.1)-(2.2).

THEOREM 3.1. *Let s and Δs be two real thresholds such that*

$$s \in]0, R_M[\quad \text{and} \quad \Delta s \in]0, R - s[. \tag{3.5}$$

Then, for all $(\rho_l, \rho_r) \in [0, R^\star]^2$, there exists a unique weak solution $(x,t) \in \mathbb{R} \times \mathbb{R}^+ \to \rho(x,t) \in [0, R^\star]$ to the Riemann problem (2.1)-(2.2)-(3.1) satisfying the following property :

The Riemann solution coincides with the classical solution unless

A. *ρ_l and ρ_r are such that (ρ_l, ρ_r) belongs to A with*

$$A = \{(\rho_l, \rho_r) \in [0, R^\star]^2 \ / \ s \leq \rho_l \leq R, \ \Phi(\rho_l) < \rho_r \leq R, \ (\rho_r - \rho_l) > \Delta s\}. \tag{3.6}$$

In this case, the Riemann solution contains an undercompressive shock connecting ρ_l to $\psi(\rho_l)$ followed by the classical Riemann solution associated with the initial states $\psi(\rho_l)$ and ρ_r.

B. *ρ_l and ρ_r are such that (ρ_l, ρ_r) belongs to B with*

$$B = \{(\rho_l, \rho_r) \in [0, R^\star]^2 \ / \ \rho_r > R, \ \rho_r > \rho_l, \ \rho_r < \psi(\rho_l)\}. \tag{3.7}$$

In this case, the Riemann solution again contains an undercompressive shock connecting ρ_l to $\psi(\rho_l)$ followed by the classical Riemann solution associated with the initial states $\psi(\rho_l)$ and ρ_r.

C. *ρ_l and ρ_r are such that (ρ_l, ρ_r) belongs to C with*

$$C = \{(\rho_l, \rho_r) \in [0, R^\star]^2 \ / \ \rho_r > R, \ \rho_r > \rho_l, \ \rho_r \geq \psi(\rho_l)\}. \tag{3.8}$$

In this case, the Riemann solution is an undercompressive shock connecting ρ_l to ρ_r.

Before addressing the numerical approximation of the solutions of (2.1)-(2.2), let us briefly comment this theorem. First of all, it is important to notice that the conditions (3.6)-(3.7)-(3.8) in the Riemann solver separate data leading to classical solutions from those generating nonclassical behaviors. Put in other words and following [11], [13] or [2], these conditions represent in some sense a *nucleation condition*, which determines

when the solution becomes nonclassical. As it may be expected, this nucleation condition will play a central part in the numerical strategy. Then, a physical interpretation may be given to situation **A.** In this case, ρ_r is sufficiently close to the border between calm and panic and ρ_l is sufficiently both large and far from ρ_r to create a panic state when facing ρ_r. An undercompressive shock between ρ_l and $\psi(\rho_l)$ expresses the corresponding violation of the usual maximum principle. In cases **B** and **C**, we have $\rho_r \in]0, R^\star]$. Thus, we observe that if $\rho_l \in [0, R]$, the two distinct regions associated with calm and panic are joined by a nonclassical behavior, using an undercompressive shock, either from ρ_l to $\psi(\rho_l)$ if possible, or from ρ_l to ρ_r otherwise. In some sense, one thus sees that the Theorem 3.1 makes the function ψ play the part of *kinetic function* as soon as possible. Finally, we refer the reader to [7] for additional properties of interest satisfied (or not) by the Riemann solver proposed in the Theorem 3.1.

4. Numerical approximation. In this section, we derive a relevant algorithm for approximating the nonclassical solutions of (2.1)-(2.2). To that purpose, the only information we rely on about the Riemann solver given in previous section is the nucleation condition (3.6)-(3.7)-(3.8). In particular, and contrarily to Godunov's scheme or Glimm's scheme for instance, we are not explicitly using the knowledge of the Riemann solutions. We follow the same approach as in [2]. The scheme is composed of two steps : an equilibrium step and a transport step. In the equilibrium step, our aim is to put at equilibrium all the admissible undercompressive discontinuities by modifying any given consistent and conservative scheme for (2.1). Then, the transport step takes into account the dynamics of these discontinuities and propagates them.

Let Δt and Δx be the time and the space steps. Introducing the interfaces $x_{j+1/2} = j\Delta x$ for $j \in \mathbb{Z}$ and the intermediate times $t^n = n\Delta t$ for $n \in \mathbb{N}$, we classicaly seek at each time t^n an approximation ρ_j^n of the solution $x \to \rho(x, t^n)$ on each interval $C_j = [x_{j-1/2}; x_{j+1/2})$, $j \in \mathbb{Z}$. The middle point of C_j is noted $x_j = 0.5\,(x_{j-1/2} + x_{j+1/2})$. In this context, we assume as given a two-point (without loss of generality) numerical flux function $(u, v) \to g(u, v)$ consistent with the flux function q, and we set $\lambda = \Delta t/\Delta x$. See also the Remark 2 below. Let us start by motivating our algorithm.

4.1. Preliminary motivation. Our scheme is designed on the following remark. A natural discretization of the Riemann initial data (3.1) consists in setting

$$\rho_j^0 = \begin{cases} \rho_l & \text{if} \quad j \leq 0, \\ \rho_r & \text{if} \quad j \geq 1. \end{cases} \tag{4.1}$$

By Theorem 3.1, we know that if (ρ_l, ρ_r) obeys (3.8), the solution is an undercompressive shock connecting ρ_l to ρ_r and propagating with speed $\sigma(\rho_l, \rho_r)$ given by the Rankine-Hugoniot jump relation :

$$\sigma(\rho_l, \rho_r) = \frac{q(\rho_r) - q(\rho_l)}{\rho_r - \rho_l}. \tag{4.2}$$

In particular, $\rho(x, t)$ always equals either ρ_l or ρ_r. From a numerical standpoint, we are tempted to take the usual conservative update formula associated with the numerical flux g, that is

$$\rho_j^{n+1} = \rho_j^n - \lambda(g_{j+1/2} - g_{j-1/2}), \quad j \in \mathbb{Z}, \tag{4.3}$$

with $g_{j+1/2} = g(\rho_j^n, \rho_{j+1}^n)$ for all $j \in \mathbb{Z}$. It gives :

$$\rho_j^1 = \begin{cases} \rho_l - \lambda(g(\rho_l,\rho_l) - g(\rho_l,\rho_l)) = \rho_l & \text{if} \quad j \leq -1, \\ \rho_l - \lambda(g(\rho_l,\rho_r) - g(\rho_l,\rho_l)) & \text{if} \quad j = 0, \\ \rho_r - \lambda(g(\rho_r,\rho_r) - g(\rho_l,\rho_r)) & \text{if} \quad j = 1, \\ \rho_r - \lambda(g(\rho_r,\rho_r) - g(\rho_r,\rho_r)) = \rho_r & \text{if} \quad j \geq 2. \end{cases}$$

with, generally speaking, $\rho_0^1 \notin \{\rho_l, \rho_r\}$ and $\rho_1^1 \notin \{\rho_l, \rho_r\}$. After the first time iteration, two intermediate states have thus been created by the conservative scheme (4.3). In order to avoid such spurious values, we are thus led to replace (4.3). We suggest this nonconservative formula :

$$\rho_j^{n+1} = \rho_j^n - \lambda(g_{j+1/2}^L - g_{j-1/2}^R), \quad j \in \mathbb{Z}, \tag{4.4}$$

where the numerical fluxes $g_{j+1/2}^L = g_{j+1/2}^L(\rho_j^n, \rho_{j+1}^n)$ and $g_{j+1/2}^R = g_{j+1/2}^R(\rho_j^n, \rho_{j+1}^n)$ have to be suitably defined. First of all, it is natural to set

$$g_{j+1/2}^L(\rho,\rho) = g_{j+1/2}^R(\rho,\rho) = g(\rho,\rho), \quad j \in \mathbb{Z},$$

for all ρ. Then, if (ρ_l, ρ_r) satisfies (3.8) with in addition $\rho_r = \psi(\rho_l)$, setting

$$g_{j+1/2}^L(\rho_l,\rho_r) = g(\rho_l,\rho_l) \quad \text{and} \quad g_{j+1/2}^R(\rho_l,\rho_r) = g(\psi(\rho_l),\rho_r), \quad j \in \mathbb{Z}, \tag{4.5}$$

is sufficient to avoid intermediate values since we get

$$\begin{cases} \rho_0^1 = \rho_l - \lambda(g_{1/2}^L(\rho_l,\rho_r) - g_{-1/2}^R(\rho_l,\rho_l)) = \rho_l - \lambda(g(\rho_l,\rho_l) - g(\rho_l,\rho_l)) = \rho_l, \\ \rho_1^1 = \rho_r - \lambda(g_{3/2}^L(\rho_r,\rho_r) - g_{1/2}^L(\rho_l,\rho_r)) = \rho_r - \lambda(g(\rho_r,\rho_r) - g(\psi(\rho_l),\rho_r)) = \rho_r. \end{cases}$$

In the same way, if (ρ_l, ρ_r) satisfies (3.8) but $\rho_r \neq \psi(\rho_l)$, setting

$$g_{j+1/2}^L(\rho_l,\rho_r) = g(\rho_l,\rho_l) \quad \text{and} \quad g_{j+1/2}^R(\rho_l,\rho_r) = g(\rho_r,\rho_r), \quad j \in \mathbb{Z}, \tag{4.6}$$

is fitting since

$$\begin{cases} \rho_0^1 = \rho_l - \lambda(g_{1/2}^L(\rho_l,\rho_r) - g_{-1/2}^R(\rho_l,\rho_l)) = \rho_l - \lambda(g(\rho_l,\rho_l) - g(\rho_l,\rho_l)) = \rho_l, \\ \rho_1^1 = \rho_r - \lambda(g_{3/2}^L(\rho_r,\rho_r) - g_{1/2}^L(\rho_l,\rho_r)) = \rho_r - \lambda(g(\rho_r,\rho_r) - g(\rho_r,\rho_r)) = \rho_r. \end{cases}$$

Thanks to the new update formula (4.4), we are thus able to remove nondesired values. Nevertheless, it is clear at this stage that the initial discontinuity (4.1) is made stationary by our new update formula. Instead, it should be moving at speed $\sigma(\rho_l, \rho_r)$ given in (4.2). This is the reason for which a transport step must be included in our algorithm. A sampling strategy will be proposed in the next section, again in order to avoid the emergence of spurious values (see just below for more details).

4.2. Transport-Equilibrium scheme. We now describe the two steps of our numerical strategy in details. As motivated in the previous subsection, the very idea is to modify the numerical flux $g_{j+1/2}(\rho_j^n, \rho_{j+1}^n)$ by means of two fluxes $g_{j+1/2}^L(\rho_j^n, \rho_{j+1}^n)$ and $g_{j+1/2}^R(\rho_j^n, \rho_{j+1}^n)$ each time that an undercompressive shock appears in the solution of the Riemann problem (2.1)-(2.2)-(3.1) associated with $\rho_l = \rho_j^n$ and $\rho_r = \rho_{j+1}^n$. According to whether this undercompressive shock connects the states ρ_j^n and $\psi(\rho_j^n)$ or not, that is depending on if $(\rho_j^n, \rho_{j+1}^n) \in A \cup B$ or $(\rho_j^n, \rho_{j+1}^n) \in C$, we will use the formulas (4.5) or (4.6) respectively. But we have shown in the previous section that

with such a modification, the undercompressive discontinuities are made stationary. Then, we will introduce a transport step in order to make moving these discontinuities with the right speed.

First step ($t^n \to t^{n+1-}$) This first step aims at making stationary the admissible undercompressive discontinuities of (2.1)-(2.2) (see Theorem 3.1). We thus consider the nonconservative version of (4.3) given by (4.4) where the numerical fluxes $g^L_{j+1/2}$ and $g^R_{j+1/2}$ are defined as follows with the aid of the nucleation condition (3.6)-(3.7)-(3.8) and for all $j \in \mathbb{Z}$:

$$g^L_{j+1/2} = \left\{ \begin{array}{ll} g(\rho^n_j, \rho^n_j) & \text{if} \quad (\rho^n_j, \rho^n_{j+1}) \in A \cup B \cup C, \\ g(\rho^n_j, \rho^n_{j+1}) & \text{otherwise,} \end{array} \right. \tag{4.7}$$

and

$$g^R_{j+1/2} = \left\{ \begin{array}{ll} g(\psi(\rho^n_j), \rho^n_{j+1}) & \text{if} \quad (\rho^n_j, \rho^n_{j+1}) \in A \cup B, \\ g(\rho^n_{j+1}, \rho^n_{j+1}) & \text{if} \quad (\rho^n_j, \rho^n_{j+1}) \in C, \\ g(\rho^n_j, \rho^n_{j+1}) & \text{otherwise.} \end{array} \right. \tag{4.8}$$

With these definitions, we easily check (see also previous subsection) that discontinuities separating two states ρ_- and ρ_+ such that $(\rho_-, \rho_+) \in C$ (that is in particular when $\rho_+ = \psi(\rho_-)$) are kept at stationary equilibrium during this first step.

Second step ($t^{n+1-} \to t^{n+1}$) This step is concerned with the dynamics of the discontinuities left stationary during the first step. Recall that the speed of propagation $\sigma(\rho_-, \rho_+)$ of a discontinuity between ρ_- and ρ_+ is given by the Rankine-Hugoniot relation (4.2). We then decide to define at each interface $x_{j+1/2}$ a speed of propagation $\sigma_{j+1/2}$:

$$\sigma_{j+1/2} = \left\{ \begin{array}{ll} \sigma(\rho^{n+1-}_j, \rho^{n+1-}_{j+1}) & \text{if} \quad (\rho^n_j, \rho^n_{j+1}) \in A \cup B \cup C, \\ 0 & \text{otherwise,} \end{array} \right. \tag{4.9}$$

and solve locally (at each discontinuity $x_{j+1/2}$) a transport equation with speed $\sigma_{j+1/2}$. If Δt is chosen sufficiently small to avoid wave interactions, we can glue together the corresponding solutions to define a solution in the whole domain. In order to get a new approximation ρ^{n+1}_j at time $t^{n+1} = t^n + \Delta t$, we propose to pick up randomly on the interval $[x_{j-1/2}, x_{j+1/2}[$ a value at time Δt in this solution. In particular, such a sampling strategy prevents the emergence of spurious intermediate values with respect to those obtained at time t^{n+1-}. Given a well distributed random sequence (a_n) within the interval $(0, 1)$, it amounts to set :

$$\rho^{n+1}_j = \left\{ \begin{array}{lll} \rho^{n+1-}_{j-1} & \text{if} & a_{n+1} \in [0, \lambda\sigma^+_{j-1/2}[, \\ \rho^{n+1-}_j & \text{if} & a_{n+1} \in [\lambda\sigma^+_{j-1/2}, 1 + \lambda\sigma^-_{j+1/2}[, \\ \rho^{n+1-}_{j+1} & \text{if} & a_{n+1} \in [1 + \lambda\sigma^-_{j+1/2}, 1[, \end{array} \right. \tag{4.10}$$

with $\sigma^+_{j+1/2} = \max(\sigma_{j+1/2}, 0)$ and $\sigma^-_{j+1/2} = \min(\sigma_{j+1/2}, 0)$ for all $j \in \mathbb{Z}$. The description of our numerical strategy is now completed.

Remark 1. - Let us consider the Riemann initial data (3.1), naturally discretized by (4.1), such that ρ_l and ρ_r are joined by an undercompressive discontinuity.

Then, the definitions of $g^L_{j+1/2}$ and $g^R_{j+1/2}$ make invisible the first step of the method ($\rho_j^{n+1-} = \rho_j^n$ for all j) and only the second step operates. This second step propagates the discontinuity using a sampling strategy. We conclude that in this particular case, our method reduces to Glimm's random choice scheme. In addition, note that the speed of propagation $\sigma(\rho_l, \rho_r)$ intervening in the second step is exact since it is calculated from the Rankine-Hugoniot relation between ρ_l and ρ_r.

- Let us now consider the Riemann initial data (3.1), again naturally discretized by (4.1), but with ρ_l and ρ_r such that the Riemann solution is classical, that is $(\rho_l, \rho_r) \notin A \cup B \cup C$. Then, $g^L_{j+1/2} = g^R_{j+1/2} = g_{j+1/2}$ and $\sigma_{j+1/2} = 0$ at each time step. In this particular case, our method thus reduces to the usual conservative scheme (4.3).

We conclude this section by highlighting the main difference between the present algorithm and the one proposed in [2]. The latter actually uses the property that the kinetic function is invertible to define $g^L_{j+1/2}$ when an undercompressive shock is present in the Riemann solution associated with the initial states ρ_j^n and ρ_{j+1}^n. More precisely and using the notations of the present paper, it writes $g^L_{j+1/2} = g(\rho_j^n, \psi^{-1}(\rho_{j+1}^n))$ instead of $g^L_{j+1/2} = g(\rho_j^n, \rho_j^n)$ in (4.7). Basically, it turns out that this definition of $g^L_{j+1/2}$ is actually crucial in [2] for obtaining good numerical results, but only in the situation when the flux is convex-concave. In this case, the undercompressive shock in the Riemann solution associated with states ρ_j^n and ρ_{j+1}^n indeed always connects the states $\psi^{-1}(\rho_{j+1}^n)$ and ρ_{j+1}^n. It is then important to involve ψ^{-1} in the definition of the numerical scheme. But in the present situation, we remark (see Theorem 3.1) that the undercompressive shocks always get ρ_j^n as left state, and then (necessarily) $\psi(\rho_j^n)$ as right state. We thus expect that the definition of $g^R_{j+1/2}$ in (4.8) involving ψ is sufficient to properly capture such discontinuities.

5. Numerical experiments. This section is devoted to the validation of the transport-equilibrium scheme we have proposed. To that purpose and without restriction, we consider a relaxation scheme as a basic numerical flux g, that is

$$g(u,v) = \frac{1}{2}(q(u) + q(v)) + \frac{a(u,v)}{2}(u - v) \quad \text{with} \quad a(u,v) = \max_{[\min(u,v),\max(u,v)]} |q'|, \tag{5.1}$$

(see [10] for instance) and we use the following standard CFL condition for computing the time step Δt at each time iteration :

$$\Delta t = \frac{1}{2} \times \frac{\Delta x}{\max_j |a(\rho_j^n, \rho_{j+1}^n)|}.$$

Remark 2. At this stage, it is important to notice that generally speaking both the numerical flux g and the time step Δt must be chosen so that the standard conservative scheme (4.3) :

(i) generates the classical solution of (2.1), in order to be relevant in situations where the solution is classical and the Transport-Equilibrium scheme simply reduces to (4.3).

(ii) obeys a discrete version of the maximum principle, that is $\forall\, n, j$ we have $\rho_j^n \in [\min_j \rho_j^0, \max_j \rho_j^0]$. Indeed, imagine that ρ_0 has the particular form (3.1) with $(\rho_l, \rho_r) \in [0, R]^2$ but $(\rho_l, \rho_r) \notin A$; the corresponding solution to (2.1) is classical by Theorem 3.1 and stays in the interval $[0, R]$. Then, if the conservative scheme (4.3) fails in satisfying a discrete maximum principle, a value $\rho_j^n > R$ may well appear for

some n, j with the (very bad) consequence of starting the nonconservative Transport-Equilibrium scheme (that is g^L and g^R no longer equal g in the whole domain) so as to generate a nonclassical solution.

Following a proposal by Collela [6], we consider the van der Corput random sequence (a_n) defined by

$$a_n = \sum_{k=0}^{m} i_k 2^{-(k+1)},$$

where $n = \sum_{k=0}^{m} i_k 2^k$, $i_k = 0, 1$, denotes the binary expansion of the integers $n = 1, 2, ...$ We easily find that the first few elements of this sequence are

$$\begin{array}{llll} a_1 = 0.5, & a_2 = 0.25, & a_3 = 0.75, & a_4 = 0.125, \\ a_5 = 0.625, & a_6 = 0.375, & a_7 = 0.875, & a_8 = 0.0625. \end{array}$$

This sequence is actually well distributed within the interval $(0, 1)$. Moreover, one can prove for instance that $a_i < 0.5$ for i even and $a_i > 0.5$ for i odd. This well-known sequence is often favourite since it leads to very good results in the smooth parts of the solutions (see [6] and [5] for an illustration).

The closure relations for the numerical simulations are as follows. First of all, the flux function q is chosen as in (2.3) (see also (2.4) and Figure 2.1 for the graphs of the functions q, ψ and Φ). Then, the thresholds s and Δs in the Theorem 3.1 are chosen to be

$$\Delta s = \Phi(0) = \frac{5}{3}, \quad s = \frac{1}{2}(R - \Delta s) = \frac{1}{6},$$

so that the condition (3.5) holds true. As last, we mention that the computations are performed on two grids, containing respectively 100 ($\Delta x = 0.01$) and 500 ($\Delta x = 0.002$) points per unit interval. Let us now consider several typical behaviors of the Riemann solution given in the Theorem 3.1. Note that the discontinuity in the Riemann initial data is still located at $x = 0$ (see (3.1)).

The first test corresponds to the choice $\rho_l = 0.5$ and $\rho_r = 1.9$, so that $(\rho_l, \rho_r) \in [0, R]^2$ but $(\rho_l, \rho_r) \notin A$ since $(\rho_r - \rho_l) < \Delta s$. The solution thus coincides with the classical one. More precisely, we observe on Figure 5.2 that it is made of a classical shock attached to a rarefaction wave.
For the Test 2, we choose $\rho_l = 0.2$ and $\rho_r = 1.9$ so that it is easily checked that $(\rho_l, \rho_r) \in [0, R]^2$ and $(\rho_l, \rho_r) \in A$. In such a situation, panic arises and the solution is composed of an undercompressive discontinuity between $\rho_l = 0.2$ and $\psi(\rho_l) \simeq 2.7744$, followed by a classical part made of a rarefaction wave and a classical shock attached to the rarefaction. We observe on Figure 5.3 that our algorithm properly captures this nonclassical solution. Note also that the undercompressive discontinuity from ρ_l to $\psi(\rho_l)$ is sharp : there is no point in the profile. For the sake of comparison, Figure 5.4 shows that the usual relaxation scheme defined by the update formula (4.3) generates a (classical) solution which lies entirely in the interval $[0, R]$ and so is far from the expected one. What proves both the need of modifying classical conservative approaches and the good design of our strategy.
In the third test case (Test 3), we choose $\rho_l = 5/2$ and $\rho_r = 1$ so that $\rho_r < \rho_l$ and the

solution is classical. On Figure 5.5, we see that the panic state ρ_l is connected to ρ_r by means of a single classical shock.
For the Test 4, we choose $\rho_l = 0.2$ and $\rho_r = 5/2$ so that $(\rho_l, \rho_r) \in B$ (recall that $\psi(\rho_l) \simeq 2.7744 > \rho_r$). By Theorem 3.1, we know that the solution is composed of an undercompressive discontinuity between ρ_l and $\psi(\rho_l)$, followed by a rarefaction wave. Here again, we observe on Figure 5.6 that our algorithm provides a numerical solution in agreement with the exact one, with in addition a sharp transition from ρ_l to $\psi(\rho_l)$. On the contrary, the usual relaxation scheme would generate a classical behavior really different from the nonclassical one (the result is not presented here).
In the fifth test case (Test 5), we take $\rho_l = 0.2$ and $\rho_r = 2.9$ so that we have now $(\rho_l, \rho_r) \in C$. By Theorem 3.1, the solution is a single undercompressive shock connecting ρ_l to ρ_r. Figure 5.7 shows that our algorithm again sharply captures this undercompressive discontinuity. Note that it and Glimm's random choice scheme are identical for this test case since the first step is clearly transparent.

Remark 3. On certain figures, some undershoots and overshoots are observed near the shocks for the q component. Recall that q is calculated as a function of ρ (the conservative unknown). They are due to the numerical diffusion of the method and to the property that the function $\rho \to q(\rho)$ is not monotone between the left and right states of the discontinuity in general. Then, depending on the densities that appear in the numerical profile of the discontinuity, an oscillation is created. Observe that having removed the numerical diffusion of the undercompressive shocks with our algorithm implies that there are not oscillations around these discontinuities.

We finish this section by giving a particular attention to the speed of propagation provided by the second step of the algorithm. This speed is calculated at each time iteration and may well vary, while in reality the speed of propagation of each undercompressive shock is constant. Let us first consider the fifth test case for which the left and right states ρ_l and ρ_r are connected by a single undercompressive discontinuity. In this case, the speed of propagation of the method is *constant* in time and rightly calculated, see the Remark 1 above. In the second and fourth test cases, the situation is different since only the left state $\rho_l = 0.2$ of the undercompressive shock is present in the initial data, but not the right state $\psi(\rho_l) \simeq 2.7744$. The latter is created by the method after some time iterations (this state behaves like an equilibrium point of the strategy) and during this process, the corresponding speed of propagation is changing to eventually reach the expected value. On Figure 5.1, we have plotted for Test 2 (Left) and Test 4 (Right) the values taken by this speed of propagation in the course of the computations (from time $t = 0$ to the final time) and for several meshes. We observe that the method only needs few time for correctly appoaching the exact speed of propagation. For instance, the relative error is around 0.01% at the final time, which explains the good results of the method.

6. Quantitative evaluation of the method. In this section, we propose to evaluate the numerical solutions obtained for the five Riemann problems we have considered above through quantitative tests. We begin with the computation of the conservation errors and then, we study the order of convergence of the method through the L^1-norm.

6.1. Conservation errors. It is obvious that our method is nonconservative since first, two numerical fluxes g^L and g^R are used in the first step and then, the transport step is based on a random sampling. We then propose to measure the

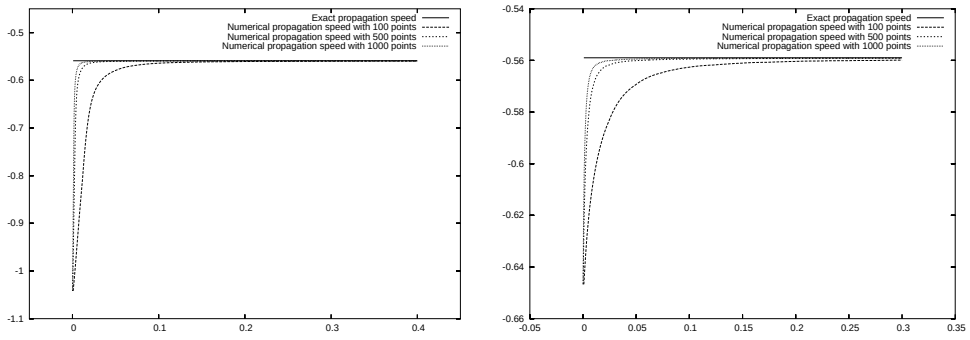

FIG. 5.1. *Numerical propagation speed of the undercompressive shock versus time : Test* 2 *(Left) and Test* 4 *(Right)*

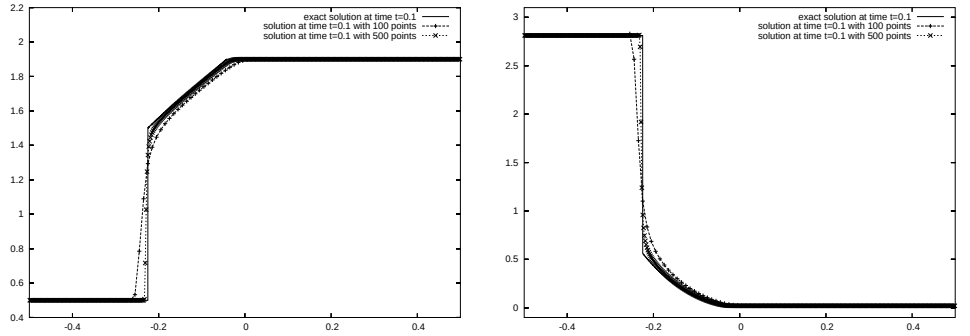

FIG. 5.2. *Test 1 - classical solution :* $x \to \rho(x)$ *(Left) and* $x \to q(\rho)(x)$ *(Right)*

conservation error on piecewise constant numerical solution ρ_λ defined as

$$\rho_\lambda(x,t) = \rho_j^n \quad \text{if} \quad (x,t) \in [x_{j-1/2}, x_{j+1/2}) \times [t^n, t^{n+1}),$$

between the times $t = 0$ and let us say $t = T > 0$. For that, we denote $[x_m, x_M]$ the computational domain and we proceed exactly as in [2] by comparing with 0 the function $E : T \in \mathbb{R}^+ \to E(T) \in \mathbb{R}$ with $E(T)$ defined by the relation

$$\int_{x_m}^{x_M} \rho_\lambda(x,T)dx \times E(T) \quad = \tag{6.1}$$

$$\int_{x_m}^{x_M} \rho_\lambda(x,T)dx - \int_{x_m}^{x_M} \rho_\lambda(x,0)dx + \int_0^T q(\rho_\lambda(x_M,t))dt - \int_0^T q(\rho_\lambda(x_m,t))dt.$$

Figures 6.1, 6.2, 6.3, 6.4 and 6.5 show the function $T \to E(T)$ for the five test cases considered in the previous section. We used $x_m = -0.5$ and $x_M = 0.5$.

For the first test case (Figure 6.1), no conservation error is made since the solution is classical so that our algorithm exactly reduces to the standard (conservative) relaxation scheme. The same happens for Test 3, see Figure 6.3.

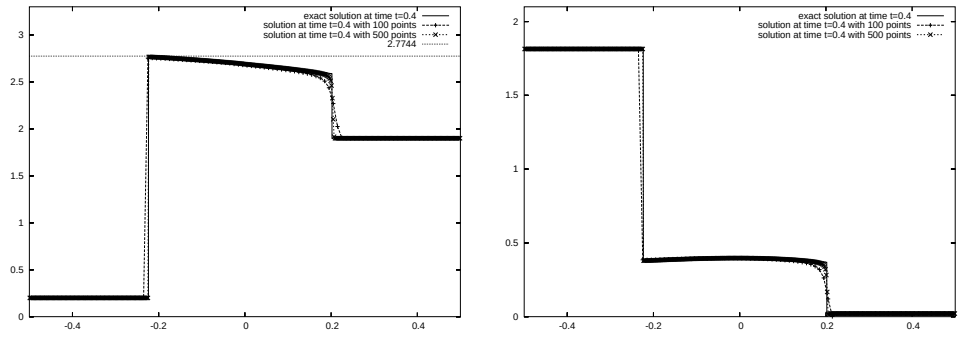

FIG. 5.3. *Test 2 - nonclassical solution : $x \to \rho(x)$ (Left) and $x \to q(\rho)(x)$ (Right)*

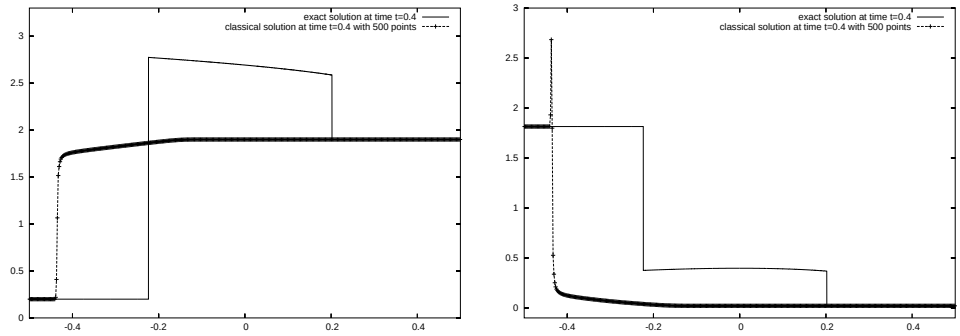

FIG. 5.4. *Test 2 - (classical) solution generated by standard relaxation method : $x \to \rho(x)$ (Left) and $x \to q(\rho)(x)$ (Right)*

In Test 2 and Test 4, for which the solution is nonclassical, we observe on Figures 6.2 and 6.4 that we have a very small conservation error : it seems to stay around 1% and 2% with 100 points in the mesh, and around 0.3% and 0.5% with 500 points in the mesh.
At last, in the last test case (Figure 6.5), we observe that the conservation error is once more low and stays around 2.2% with 100 points and around 0.5% with 500 points.

To conclude this section, we now address this lack of conservation in term of the number of pedestrians. Let us first notice that the exact solution obeys

$$0 = \int_{x_m}^{x_M} \rho(x,T)dx - \int_{x_m}^{x_M} \rho(x,0)dx + \int_0^T q(\rho(x_M,t))dt - \int_0^T q(\rho(x_m,t))dt,$$

so that provided the dynamics of the numerical solution has not reached x_m and x_M (which means $q(\rho_\lambda(x_m,t)) = q(\rho(x_m,t))$ and $q(\rho_\lambda(x_M,t)) = q(\rho(x_M,t))$) we get

$$E(T) = \frac{\displaystyle\int_{x_m}^{x_M} \rho_\lambda(x,T)dx - \int_{x_m}^{x_M} \rho(x,T)dx}{\displaystyle\int_{x_m}^{x_M} \rho_\lambda(x,T)dx}.$$

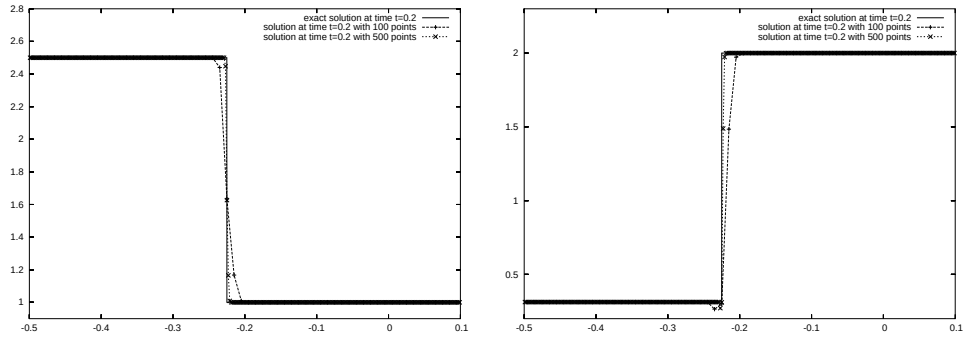

FIG. 5.5. *Test 3 - classical solution : $x \to \rho(x)$ (Left) and $x \to q(\rho)(x)$ (Right)*

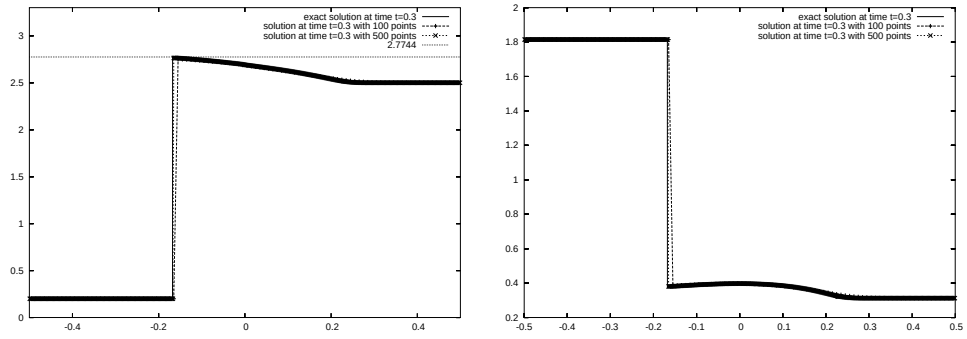

FIG. 5.6. *Test 4 - nonclassical solution : $x \to \rho(x)$ (Left) and $x \to q(\rho)(x)$ (Right)*

Then, $E(T)$ represents the relative conservation error of ρ at time T on the interval $[x_m, x_M]$ and $\displaystyle\int_{x_m}^{x_M} \rho_\lambda(x,T)dx \times E(T)$ gives the number of persons lost in each computation. At the final time, we found this number equals 0.0097, -0.0203 and -0.0169 for Tests 2, 4 and 5 respectively (and for 100 points only). This represents only a small portion of a person. Since to get integer numbers of people we have to round these results, we then eventually recover the conservation property (nobody is lost).

6.2. Convergence rate. We now investigate numerically the convergence rate of the method for all the Riemann problems considered until now. We measure the L^1-norm E_{L^1} of the difference between the exact and the numerical solution by the following usual formula :

$$E_{L^1} = \Delta x \sum_{j \in \mathbb{Z}} |\rho_\lambda(x_j, T_f) - \rho(x_j, T_f)|,$$

where T_f is the final time of the computation. This quantity is evaluated for several space steps Δx and the results are presented on a graph relating $\ln(E_{L^1})$ to $\ln(\Delta x)$. Figure 6.6 - Left is concerned with Tests 1 and 3 for which the solutions are classical. In this case, we have already underlined (see the Remark 1) that our algorithm is equivalent to the conservative scheme given by the numerical flux g. Then, what we

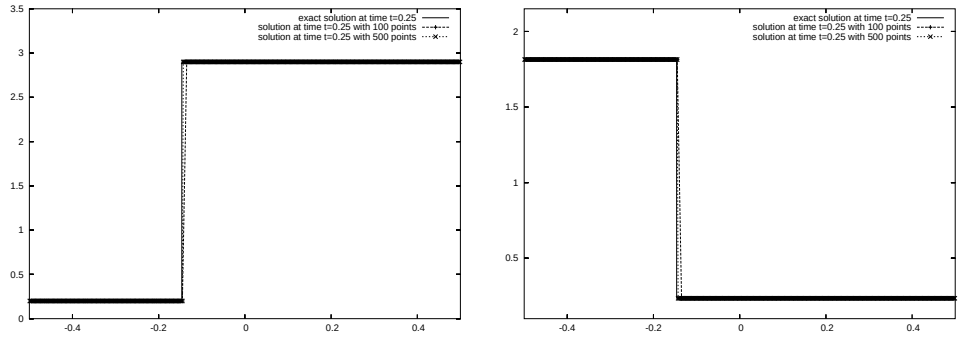

FIG. 5.7. *Test 5 - nonclassical solution : $x \to \rho(x)$ (Left) and $x \to q(\rho)(x)$ (Right)*

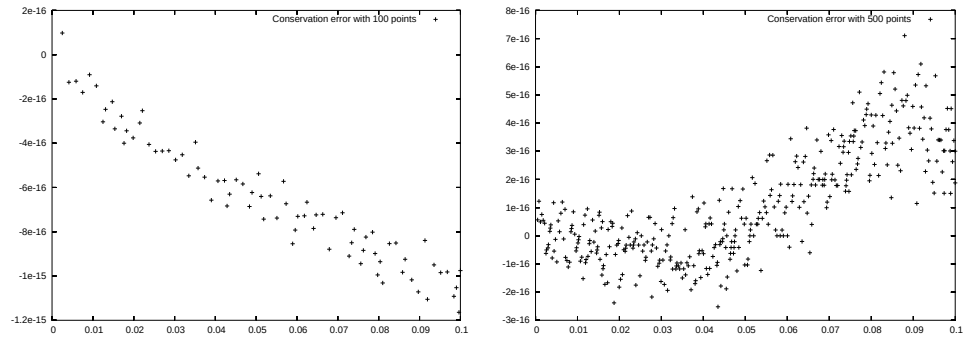

FIG. 6.1. *Test 1 - conservation error with* 100 *(Left) and* 500 *(Right) points in the mesh*

are measuring here is nothing but the convergence rate of the numerical solution to the exact solution for the relaxation scheme (5.1). The meshes we have used contain $2^i \times 500$ nodes per unit interval, with an integer i varying from 0 to 5. The solution of Test 3 is a pure classical shock and we obtain a convergence rate of approximately 0.999. On the contrary, for Test 1 the solution is a classical shock followed by an attached rarefaction wave. The convergence rate observed for this *compound* wave is around 0.845 and then is less than for the pure shock.
Figure 6.6 - Right shows the results for Tests 2, 4 and 5 for which the solutions develop an undercompressive shock. The meshes now contain $2^i \times 500$ nodes per unit interval, with i varying from 0 to 6. Let us begin with Test 5. The solution is a pure undercompressive shock and our method is identical to Glimm's random choice scheme in this case (see again the Remark 1). We get a convergence rate of 1 which is expected for this scheme. For Tests 2 and 4 the patterns of the solutions are more complicated since the undercompressive shock is not pure anymore but attached to a rarefaction wave. Around this undercompressive discontinuity, our method then actually blends Glimm's random choice scheme and the relaxation scheme. We observe that the experimental order of convergence for Test 2 is close to 1, while for Test 4 it is not yet established but the convergence seems secured.

7. Conclusion. We have proposed a very efficient numerical strategy for computing the nonclassical solutions of a particular non genuinely nonlinear scalar con-

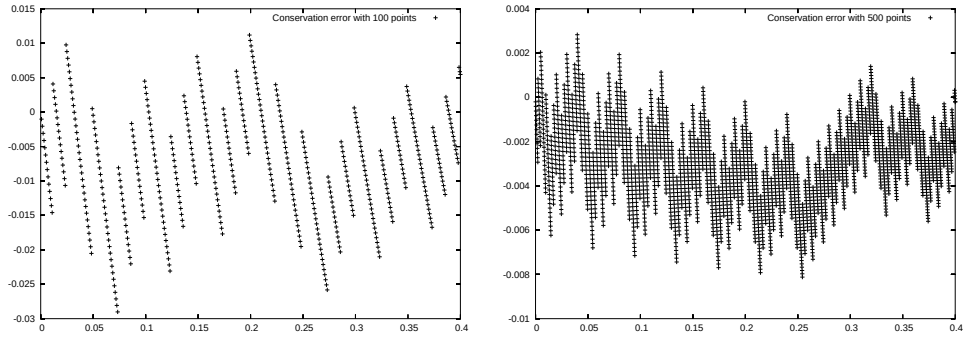

FIG. 6.2. *Test 2 - conservation error with* 100 *(Left) and* 500 *(Right) points in the mesh*

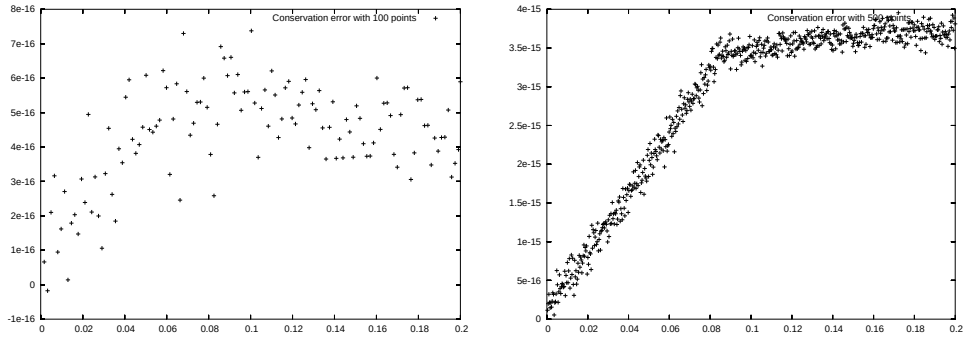

FIG. 6.3. *Test 3 - conservation error with* 100 *(Left) and* 500 *(Right) points in the mesh*

servation law (q is neither convex nor concave), recently introduced by Colombo and Rosini [7] for simulating human flows. The validation has been (successfully) carried out past several relevant Riemann initial data. The fact is that our approach is non-conservative, but measurements have shown that the loss of mass is extremely low, while the numerical solutions fully agree with the exact ones. Now it would be of interest to use the method past initial data associated with concrete situations.

REFERENCES

[1] Chalons C., *Bilans d'entropie discrets dans l'approximation numérique des chocs non classiques. Application aux équations de Navier-Stokes multi-pression 2D et à quelques systèmes visco-capillaires*, PhD Thesis, Ecole Polytechnique, (2002).

[2] Chalons C., *Transport-Equilibrium Schemes for Computing Nonclassical Shocks. I. Scalar Conservation Laws*, Preprint of the Laboratoire Jacques-Louis Lions (2005).

[3] Chalons C. et LeFloch P.G., *A fully discrete scheme for diffusive-dispersive conservation laws*, Numerisch Math., vol 89, pp 493-509 (2001).

[4] Chalons C. et LeFloch P.G., *High-order entropy conservative schemes and kinetic relations for van der Waals fluids*, J. Comput. Phys., vol 167, pp 1-23 (2001).

[5] Chalons C. and LeFloch P.G., *Computing undercompressive waves with the random choice scheme. Nonclassical shock waves*, Interfaces and Free Boundaries, vol 5, pp 129-158 (2003).

[6] Collela P., *Glimm's method for gas dynamics*, SIAM J. Sci. Stat. Comput., vol 3, pp 76-110 (1982).

[7] Colombo R.M. and Rosini M.D., *Pedestrian Flows and Nonclassical Shocks*, Mathematical Methods in the Applied Sciences, vol 28, issue 13, pp 1553-1567 (2005).

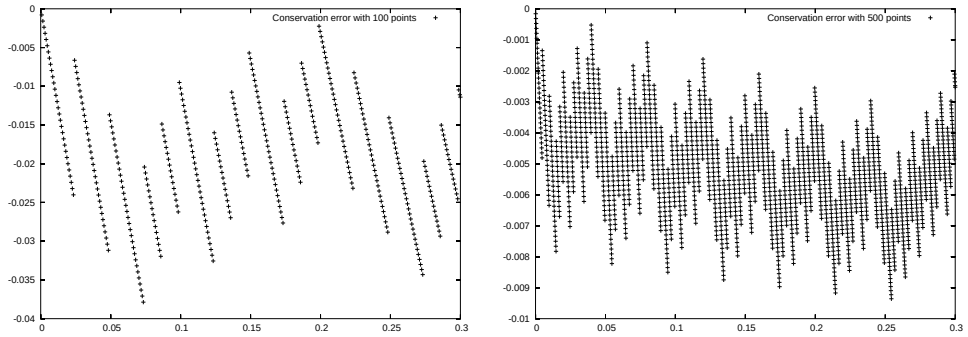

FIG. 6.4. *Test 4 - conservation error with* 100 *(Left) and* 500 *(Right) points in the mesh*

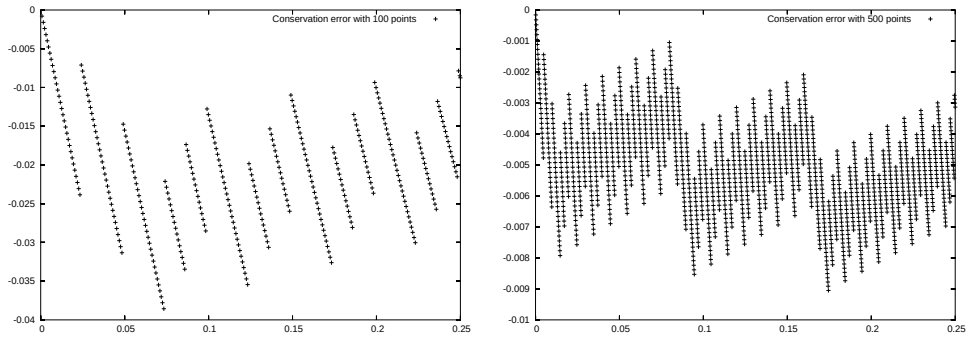

FIG. 6.5. *Test 5 - conservation error with* 100 *(Left) and* 500 *(Right) points in the mesh*

[8] Hayes B.T. and LeFloch P.G., *Nonclassical shocks and kinetic relations : Scalar conservation laws*, Arch. Rational Mech. Anal., vol 139, pp 1-56 (1997).
[9] Hayes B.T. and LeFloch P.G., *Nonclassical shocks and kinetic relations : Finite difference schemes*, SIAM J. Numer. Anal., vol 35, pp 2169-2194 (1998).
[10] Lattanzio C. and Serre D., *Convergence of a relaxation scheme for hyperbolic systems of conservation laws*, Numer. Math., vol 88, pp 121-134 (2001).
[11] LeFloch P.G., **Hyperbolic Systems of Conservation Laws: The theory of classical and nonclassical shock waves**, E.T.H. Lecture Notes Series, Birkhäuser (2002).
[12] LeFloch P.G. and Rohde C., *High-order schemes, entropy inequalities, and nonclassical shocks*, SIAM J. Numer. Anal., vol 37, pp 2023-2060 (2000).
[13] LeFloch P.G. and Shearer M., *Nonclassical Riemann solvers with nucleation*, Proc. Royal Soc. Edinburgh, vol 134A, pp 941-964 (2004).
[14] Lighthill M.J. and Whitham G.B., *On kinematic waves. II. A theory of traffic flow on long crowded roads*, Proc. Royal Soc. London, Ser. A., vol 229, pp 317-345 (1955).
[15] Liu T.P., *Admissible solutions of hyperbolic conservation laws*, Amer. Math. Soc., vol 30 (1981).
[16] Richards P.I., *Shock waves on the highway*, Operations Res., vol 4, pp 42-51 (1956).

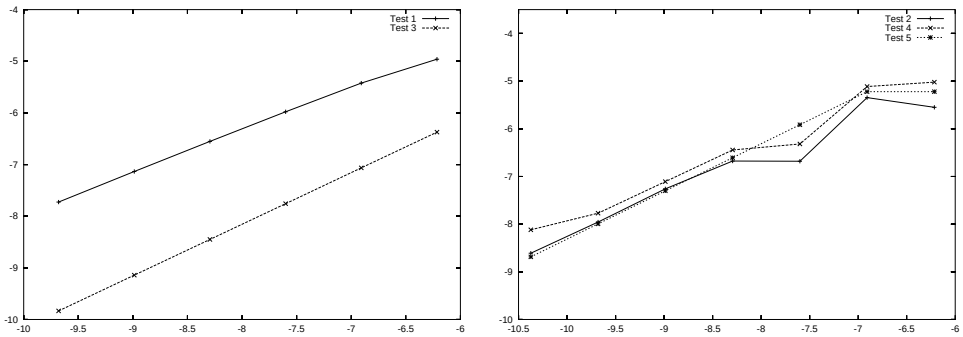

FIG. 6.6. $\ln(E_{L^1})$ *versus* $\ln(\Delta x)$